JOURNAL OF MATERIALS SCIENCE 16 (1981) 1895–1908

The effect of aluminium on mechanical properties and thermal stability of (Fe,Co,Ni)–Al–B ternary amorphous alloys

A. INOUE, A. KITAMURA,* T. MASUMOTO
The Research Institute for Iron, Steel and Other Metals, Tohoku University, Sendai 980, Japan

Amorphous phase formation has been found in a wide range of Fe–Al–B, Co–Al–B and Ni–Al–B ternary systems by a melt-quenching technique. The aluminium content of these amorphous alloys is in the range 0 to 60 at % for Fe– and Co–Al–B systems and 0 to 26 at % for the Ni–Al–B system, but the formation of ductile amorphous phase is limited to less than 20 at % Al. Crystallization temperature and Vickers hardness increase with increasing aluminium and boron content and maximum values are attained at 887 K and 880 diamond pyramid number (DPN). Their fracture strengths are about 2140 to 2680 MPa. The effectiveness of aluminium on the increase in crystallization temperature and hardness is greater in the case of other metal elements such as chromium, manganese, iron, cobalt and nickel, but is less than the metalloid elements such as silicon and boron. This could be reasonably explained by the assumption that aluminium may also possess a weak metalloid character.

1. Introduction

The transition metals iron, cobalt and nickel containing metalloid elements such as boron, carbon, silicon and phosphorus are the most widely-studied family of amorphous alloys. This type of amorphous alloy is relatively easy to quench from the melt and their mechanical and magnetic properties are sufficiently excellent to warrant commercial exploitation.

In addition to these metalloid elements, aluminium has been considered to possess a considerably strong metalloid-like character. Up till now, however, systematic information about the effect of aluminium on the formation and properties of amorphous alloys has not been obtained in spite of their high engineering potential resulting from their low cost as well as the ease with which aluminium-containing alloys may be melted and ejected. From this point of view, the present authors have recently performed a series of investigations [1–4] on the melt-quenched structure of alloys containing aluminium and have found that a completely amorphous phase is formed in a wide composition range for X–Al–B (X = Fe, Co or Ni) systems. The aim of this paper is to present the formation range, crystallization behaviour and mechanical properties of amorphous alloys in these systems and to clarify the effect of aluminium on their properties.

2. Experimental methods

The specimens used in the present work were $Fe_xAl_yB_z$, $Co_xAl_yB_z$ and $Ni_xAl_yB_z$ ternary alloys. These subscripts are weighed values and represent atomic percentages. Mixtures of electrolytic pure metal (iron, cobalt or nickel), aluminium (99.99 wt %) and boron (99.8 wt %) containing 0.03 wt % Fe and 0.01 wt % C etc. impurities were melted in a flowing argon atmosphere using an induction furnace. The melts were sucked into a quartz tube of about 3 mm inner diameter and solidified in the tube. Continuous ribbon speci-

*Present address: The Patent Bureau, Tokyo 100, Japan.

0022–2461/81/071895–14$03.40/0

mens of 1 to 2 mm width and 0.02 to 0.03 mm thickness were prepared by directing a stream of molten alloy onto the outer surface of a rapidly revolving steel or copper roller. The copper roller was employed only for preparation of nickel-based alloys.

The as-quenched phases and their structural changes upon heating were examined by conventional X-ray diffraction methods using filtered FeKα and CuKα radiation and transmission electron microscopy. The transmission electron microscope samples were electrolytically thinned in an electrolyte consisting of 90 parts ethyl alcohol and 10 parts perchloric acid, the electrolyte being cooled to approximately 273 K. Hardness and fracture strength were measured with a Vickers microhardness tester using a 100 g load and an Instron-type tensile testing machine at a strain rate of 1.7×10^{-4} sec^{-1}. The crystallization temperature of the alloys was measured by a differential thermal analyser (DTA) at a heating rate of 8.33×10^{-2} K sec^{-1} and the activation energy for crystallization was examined by a differential scanning calorimeter (DSC) at various heating rates ranging from 8.33×10^{-2} to 1.33 K sec^{-1}. The ductile–brittle transition behaviour was tested for the specimens annealed for various periods at 573 K in evacuated silica capsules. Ductility was evaluated by measuring the radius of curvature at fracture in a simple bend test.

3. Results and discussion

3.1. Formation ranges of the amorphous phase and crystallization temperature

Formation of a completely amorphous phase was achieved for a wide range of compositions in the Fe–Al–B, Co–Al–B and Ni–Al–B ternary systems as shown in Figs 1 to 5. The values in the figures are the crystallization temperatures determined as the starting point of the first exothermic peak on the DTA curves. A completely amorphous phase was obtained in a very wide range of compositions, e.g. 0 to 60 at % Al for Fe– and Co–Al–B alloys and 0 to 26 at % Al for Ni–Al–B alloys. No amorphous single phase was found in the aluminium-rich composition range for the Ni–Al–B system. However, ductile amorphous alloys showing complete bending are limited to less than about 12 at % Al for Fe–Al–B, 16 at % Al for Co–Al–B and 20 at % Al for Ni–Al–B as seen in the figures. Thus, the formation range of ductile amorphous alloys becomes narrower for the nickel, cobalt and iron systems in that order. Although the reason for the ductile to brittle transition observed with increasing aluminium content is not clear at present, it may be due to the following two facts: (1) the dissolution of aluminium results in the generation of a large internal strain because of the large difference in atomic size between iron, cobalt or nickel and aluminium, and (2) aluminium possesses a favourable atomic

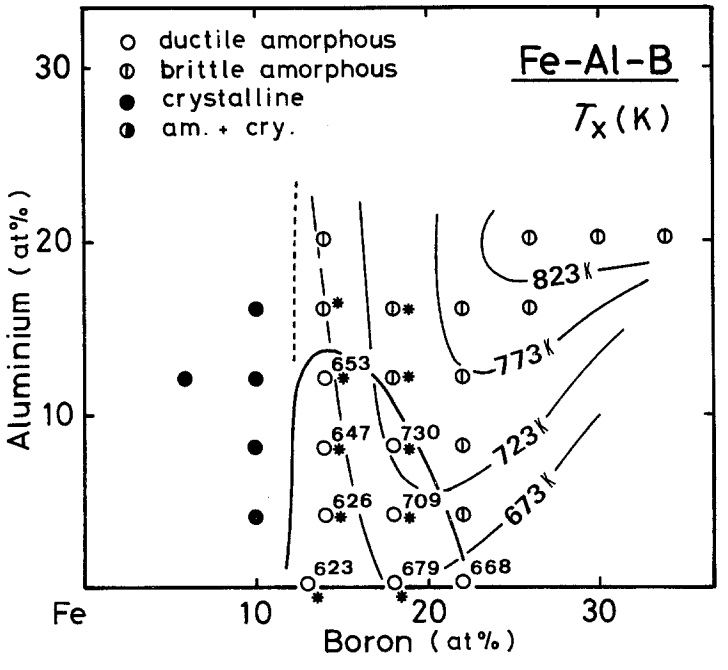

Figure 1 Composition range for the formation of amorphous phase and the change of crystallization temperature (T_x) in the iron-rich composition range for the Fe–Al–B system.

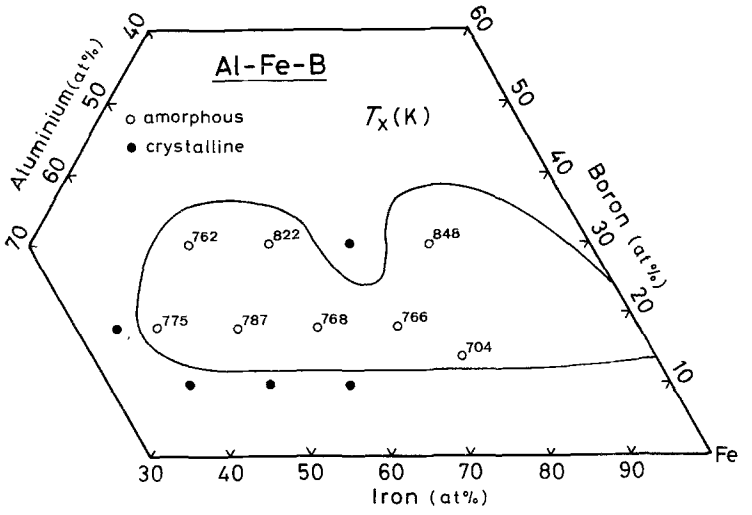

Figure 2 Composition range for the formation of amorphous phase and the change of crystallization temperature (T_x) in the aluminium-rich composition range for the Fe–Al–B system.

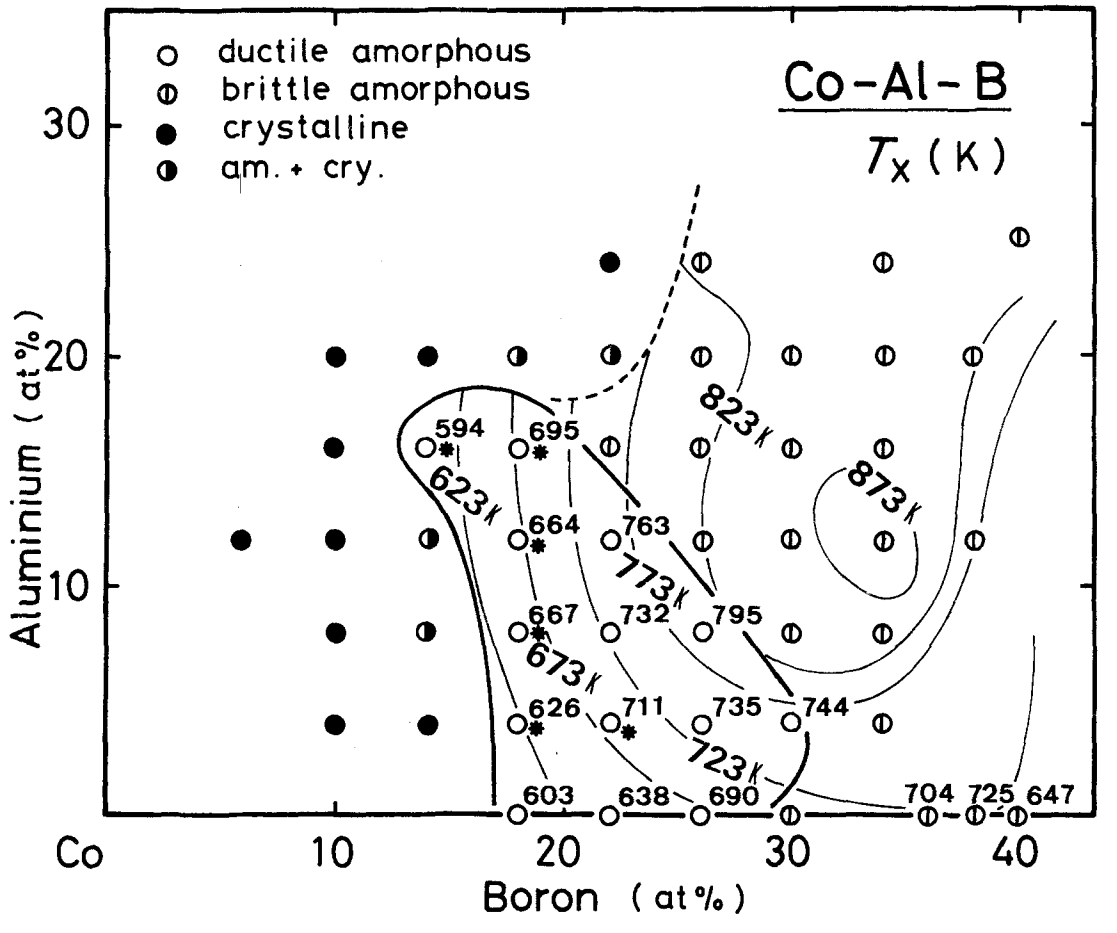

Figure 3 Composition range for the formation of amorphous phase and the change of crystallization temperature (T_x) in the cobalt-rich composition range for the Co–Al–B system.

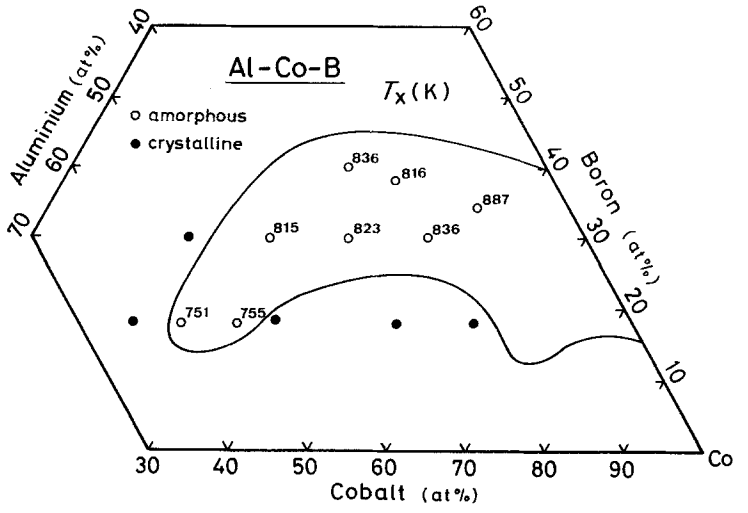

Figure 4 Composition range for the formation of amorphous phase and the change of cystallization temperature (T_x) in the aluminium-rich composition range for the Co–Al–B system.

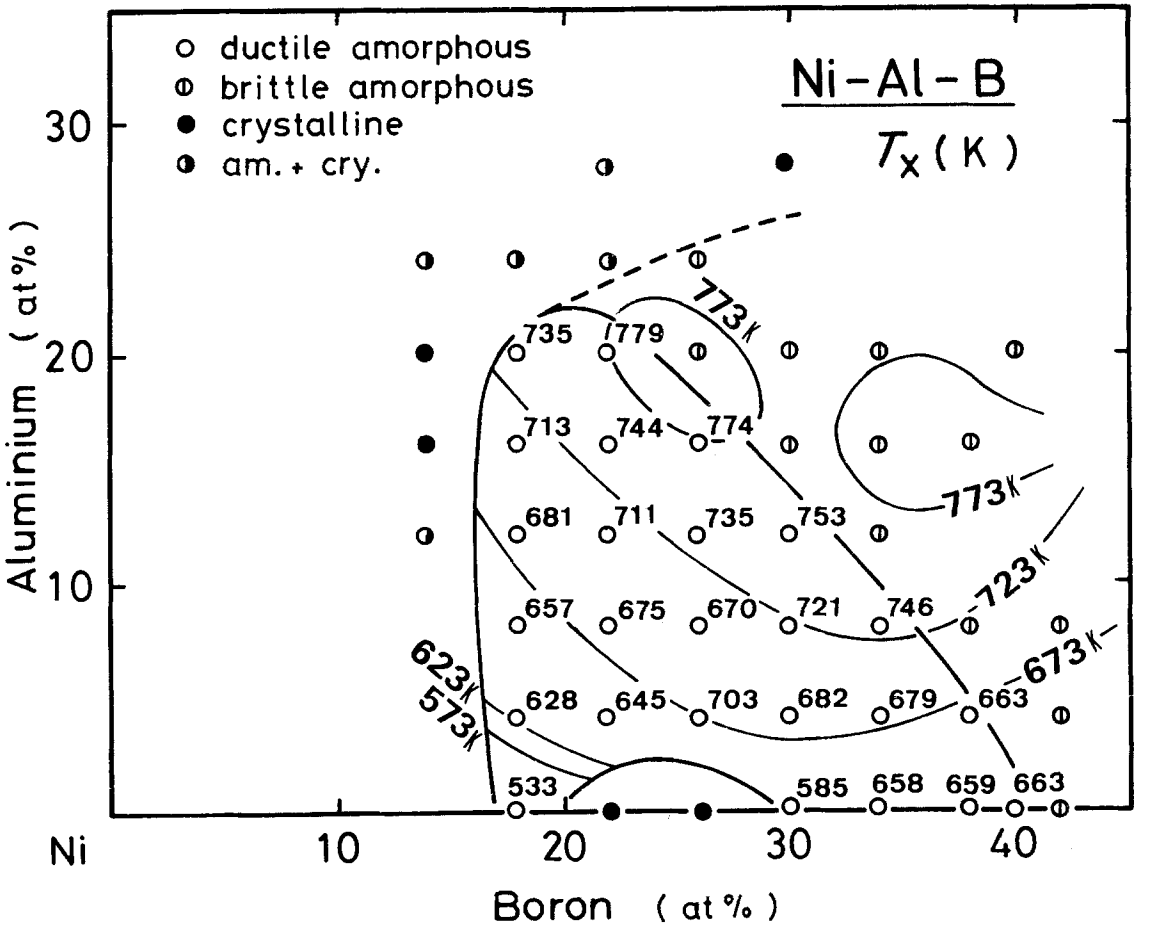

Figure 5 Composition range for the formation of amorphous phase and the change of crystallization temperature (T_x) in the nickel-rich composition range for the Ni–Al–B system.

size and electrochemical factor for the generation of a strong interaction between iron, cobalt or nickel and aluminium. The possibility of the strong interaction between both atoms is also seen from the easy formation of the superlattice structure for crystalline (Fe, Co or Ni)–Al binary alloys [5] because of a tendency for aluminium atoms to avoid being close neighbours. In this way the strain energy resulting from the close contact of relatively large solute aluminium atoms is reduced.

Judging from the equilibrium phase diagrams of X–B and X–Al (X = Fe, Co or Ni) [5] binary and X–Al–B (X = Co or Ni) [6, 7] ternary systems, the formation ranges of amorphous phase seem to be located around the deep eutectic troughs where the melting point is low. As seen in Figs 1 to 5, amorphous phase formation in the Fe–B, Co–B and Ni–B binary systems is relatively easy, whereas no amorphous phase is formed in X–Al (X = Fe, Co or Ni) binary alloys. The amorphous forming range of the Ni–Al–B system (Fig. 5) represents the results obtained with a melt-spinning apparatus with a copper roller as described in Section 2 and is much wider compared with the previous results [8] obtained with a steel roller. Thus, the amorphous forming range depends largely on the difference in the imposed cooling rate due to the specimen thickness and the roller material.

The composition ranges of the amorphous phase in X–Al–B (X = Fe, Co or Ni) systems are much wider than those in the analogous alloy systems such as X–Si–B [9, 10], Fe–P–B [11] and Fe–C–B [11]. The wide amorphous phase formation range is due to the amorphous phase formation in aluminium rich regions. Here, the reason for the formation of the amorphous alloys containing a large amount of aluminium will be considered briefly. As seen in Figs 1, 3 and 5, the replacement of iron, cobalt or nickel with aluminium appears to have little influence on the extension of their amorphous forming ranges in (Fe, Co or Ni)–B alloys. That is, the boron concentration for the formation of amorphous phase is almost constant except for $Co_{70}Al_{14}B_{16}$ and $Ni_{72-78}B_{22-28}$ alloys in the comparison between (Fe, Co or Ni)–B binary and (Fe, Co or Ni)–Al–B ternary alloys. Additionally, aluminium has a much larger atomic size compared with iron, cobalt or nickel. These results suggest that aluminium possesses the metal-like character in the amorphous phase of these systems and might dissolve substitutionally. As a result, the direct contact of aluminium–aluminium atoms is easily permitted in the amorphous state similar to other common metal atoms [12], resulting in the formation of amorphous alloys containing a large amount of aluminium. This inference also receives support from the fact that aluminium rich amorphous phases containing more than about 50 at% aluminium are obtained in many alloy systems such as Al–Cu [13], Al–Si [13], Al–Ge [14, 15], Al–Ni [15], Al–Pd [13, 15] and Al–Fe–Si [16].

The crystallization temperature T_x rises gradually with increasing aluminium and/or boron content, and reaches 848 K for $Fe_{50}Al_{20}B_{30}$, 887 K for $Co_{54}Al_{12}B_{34}$ and 795 K for $Ni_{54}Al_{20}B_{26}$ and then tends to decrease with a further increase in aluminium content. This indicates that the amorphous phase of the iron- and cobalt-based alloys is thermally more stable than that of the nickel-based alloys. Also, the most stable alloys against crystallization are located on the boron-rich side in the amorphous forming regions. One can see that the effect of aluminium on the increase of T_x is slightly less than that of boron.

3.2. Crystallization behaviour

Changes in the exothermic peak on the DTA curve were examined for Fe–, Co– and Ni–Al–B amorphous alloys. The general features of the DTA curves for Fe–Al–B alloys are shown in Fig. 6. A broad, low intensity peak on the low temperature side results from the precipitation of the first crystalline phase from the amorphous phase and a narrow, high intensity peak on the high temperature side is due to the transition of the remaining amorphous phase to the second crystalline phase. With increasing total metalloid content, the broad peak shifts toward the higher temperatures and it becomes less exothermic. At about 22 at%, this peak disappears and only the sharp peak remains, indicating the direct appearance of the second phase from the amorphous phase. The asterisks in Figs 1, 3 and 5 represent the existence of two peaks on the DTA curves. This range is limited to less than about 18 at% B for the Fe–Al–B system and about 22 at% B for the Co–Al–B system. For the Ni–Al–B system all the alloys exhibit only the sharp peak. This tendency indicates that the precipitation of the first crystalline phase is retarded with increasing boron content, while that of the second crystalline phase is hardly changed.

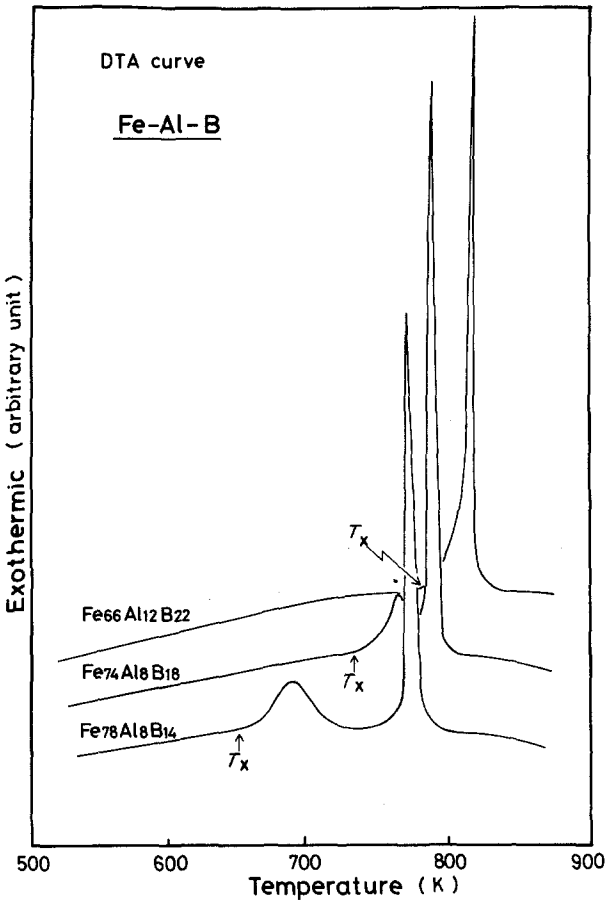

Figure 6 Differential thermal analysis curves for several Fe–Al–B amorphous alloys.

The activation energy for crystallization was determined from the exothermic peak on the DSC curve by the Kissinger method [17]. As shown in Fig. 7, a linear relationship exists between $\ln(\Phi/T_p^2)$ and $1/T_p$, where Φ is the heating rate and T_p the temperature of the exothermic peak. Also, in the figure, the data of the $Ni_{75}Si_8B_{17}$ amorphous alloy containing almost the same amount of metalloids are plotted for comparison. The activation energy for crystallization is estimated to be about 240 kJ mol^{-1} for $Fe_{74}Al_8B_{18}$, 220 kJ mol^{-1} for $Co_{74}Al_8B_{18}$ and 180 kJ mol^{-1} for $Ni_{74}Al_8B_{18}$. The energy decreases in the order Fe–, Co– to Ni–Al–B alloy, similar to the order of crystallization temperature. It is well known that the crystallization of amorphous alloys occurs by a nucleation and growth process which is controlled by the diffusion of base metal. Judging from the fact that the activation energies for self-diffusion are 254, 268 and 281 kJ mol^{-1} for Fe, Co and Ni [18], respectively, and are larger compared with the activation energies of crystallization, the diffusion of atoms in Fe–, Co– and Ni–Al–B amorphous alloy appears to be easier compared with the crystalline alloys. Further, one can see in Fig. 7 that the activation energy of crystallization of $Ni_{74}Si_8B_{18}$ amorphous alloy (180 kJ mol^{-1}) is much lower than that of $Ni_{75}Si_8B_{17}$ amorphous alloy (335 kJ mol^{-1}). This result indicates that the Ni–Al–B alloy is more unstable with respect to heating compared with the Ni–Si–B alloy. Therefore it may be stated that the diffusion of atoms in amorphous alloys differs significantly with the type of metalloid elements present.

In order to examine in more detail the precipitation behaviour of the first and second crystalline phases from the amorphous phase, observations of structural changes in X–Al–B amorphous alloys upon heating were performed by transmission electron microscopy. Fig. 8 shows the morphology and crystalline structure of the first and the second phases for $Fe_{78}Al_8B_{14}$, $Co_{66}Al_{16}B_{18}$ and $Ni_{62}Al_{20}B_{18}$ amorphous alloys heated for different periods of time at various temperatures. As seen in the photographs, the crystalline phase with a circular or elliptical morphology precipitates first

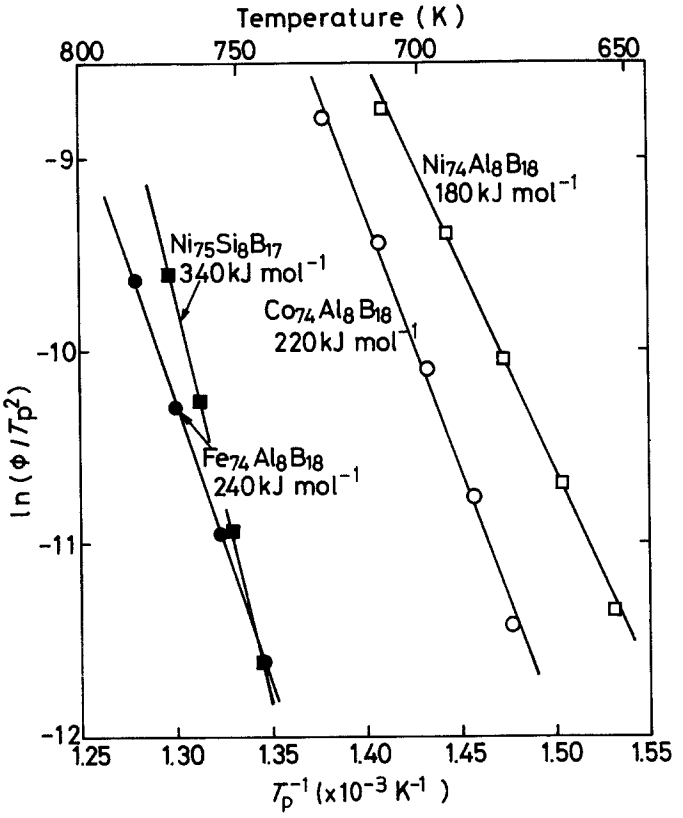

Figure 7 Kissinger plots of $\ln(\Phi/T_p^2)$ against $1/T_p$ for $Fe_{74}Al_8B_{18}$, $Co_{74}Al_8B_{18}$ and $Ni_{74}Al_8B_{18}$ amorphous alloys.

and heating at higher temperatures induces a change from the remaining amorphous phase to another crystalline phase. The first precipitate is iron crystals with a b c c structure for the Fe–Al–B system, cobalt crystals with an h c p structure for the Co–Al–B system and nickel crystals with a f c c structure for the Ni–Al–B system. On the other hand, the crystal structure of the second precipitate could not be really determined from analyses of diffraction patterns, but this phase looks like a compound containing large amounts of aluminium and boron. Such a crystallization process via two stages (Amorphous → Amorphous + Crystal-I → Crystal-I + Crystal-II) for X–Al–B (X = Fe, Co or Ni) amorphous alloys is quite similar to that for X–Si–B (X = Fe, Co or Ni) amorphous alloys [9, 10].

3.3. Mechanical properties and embrittlement behaviour by ageing

The Vickers hardness (H_v) and tensile fracture strength (σ_f) of Fe–Al–B, Co–Al–B and Ni–Al–B amorphous alloys with a good bend ductility are shown in Figs 9 to 11, wherein the values marked with an asterisk are the tensile fracture strength expressed in units of MPa. As seen in these figures, H_v increases gradually with the amount of aluminium or boron present and reaches about 730 DPN for $Fe_{78}Al_4B_{18}$, 880 DPN for $Co_{66}Al_8B_{26}$ and 875 DPN for $Ni_{58}Al_{12}B_{30}$. Thus, the higher hardness is obtained near the aluminium- or boron-rich side of the amorphous forming region. Also, the fracture strengths are about 2680 MPa for $Ni_{74}Al_8B_{18}$, about 2230 MPa for $Co_{74}Al_8B_{18}$ and about 2140 MPa for $Ni_{74}Al_8B_{18}$. These strength values are of the same order as those for X–Si–B (X = Fe, Co or Ni) alloys [19] reported previously. The mean value of H_v/σ_f is about 2.8, similar to those of a number of amorphous alloys [20]. This implies that the amorphous alloys containing a large amount of aluminium also exhibit plastic–rigid behaviour [21]. Tensile fracture occurred on the shear plane at about 50° to the tensile axis in the direction of thickness, and the fracture surface consisted of a smooth part produced by shear slip and a vein-like part produced by plastic instability, similar to the characteristics of the fracture morphology for metal–metal and metal–metalloid amorphous alloys. In comparison with the hardness values (H_v) and fracture strengths (σ_f) among

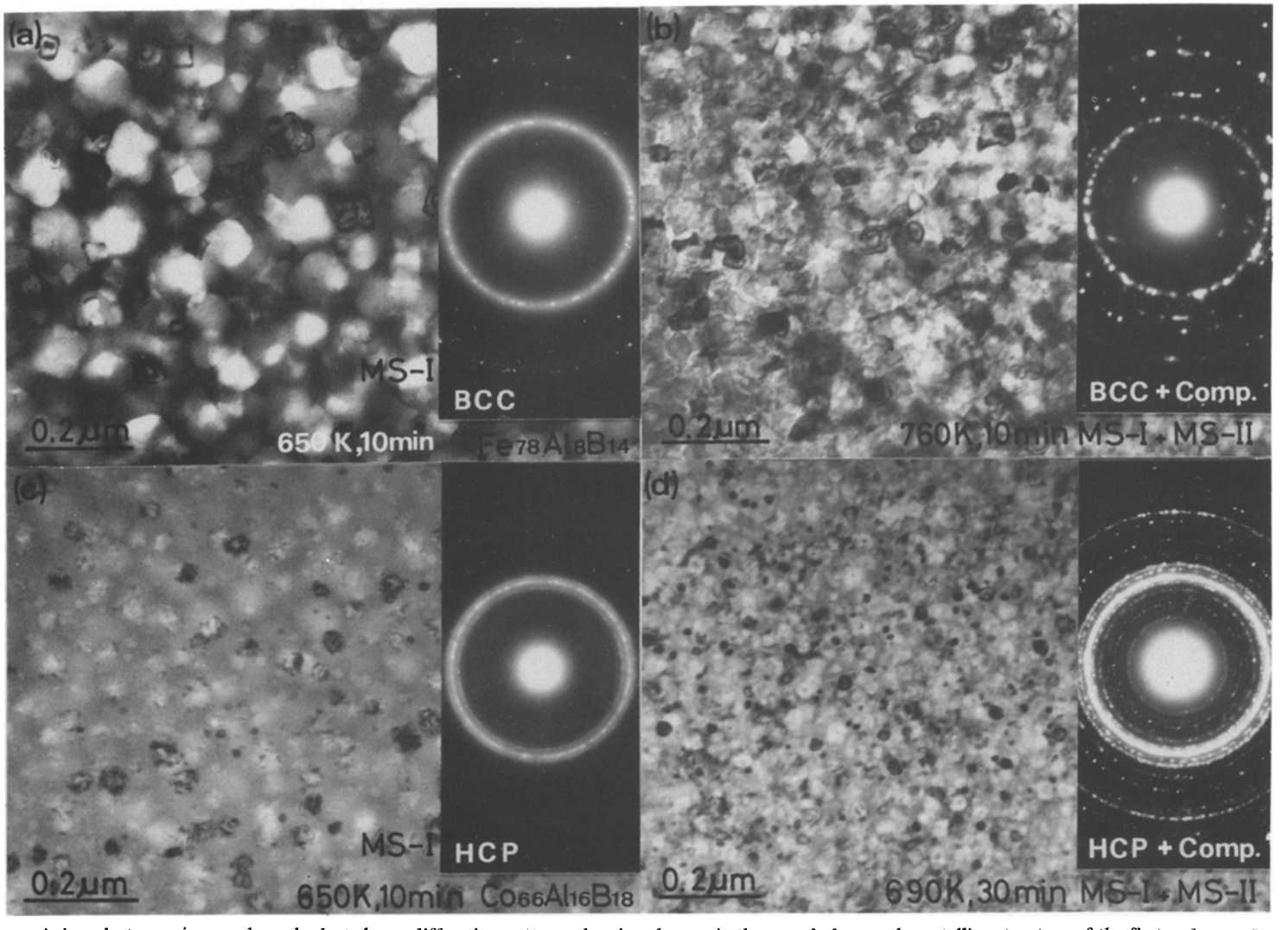

Figure 8 Transmission electron micrographs and selected area diffraction patterns showing changes in the morphology and crystalline structure of the first and second precipitates for $Fe_{78}Al_8B_{14}$, $Co_{66}Al_{16}B_{18}$ and $Ni_{62}Al_{20}B_{18}$ amorphous alloys.

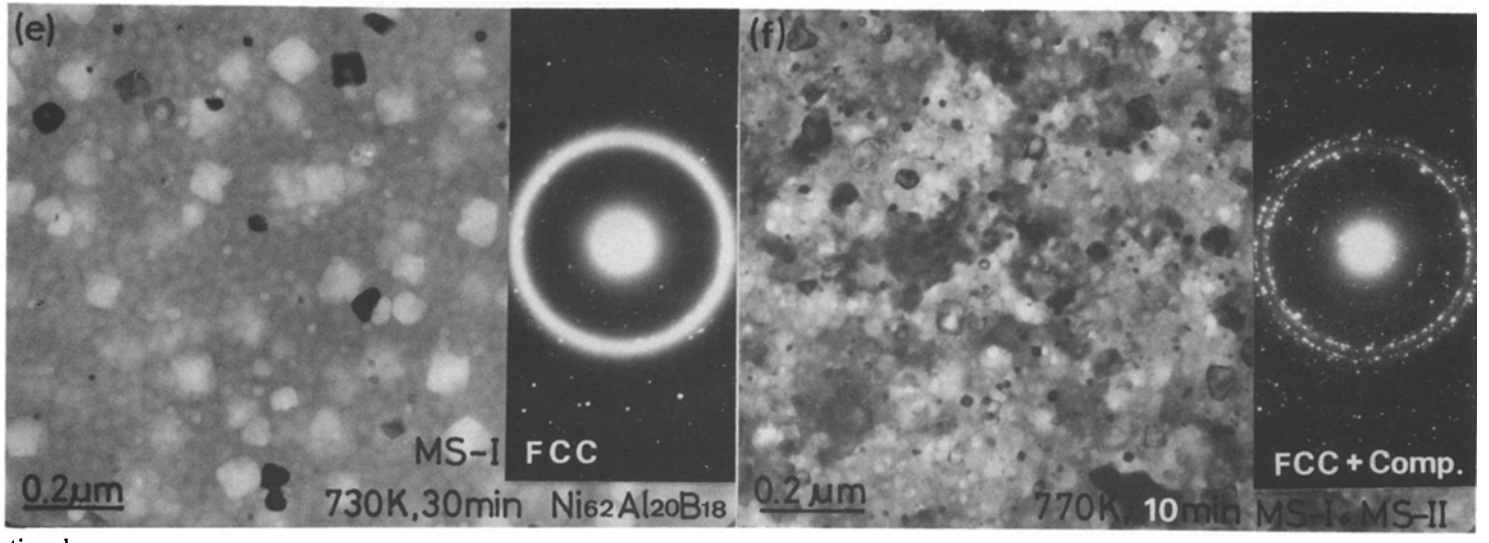

Figure 8 Continued.

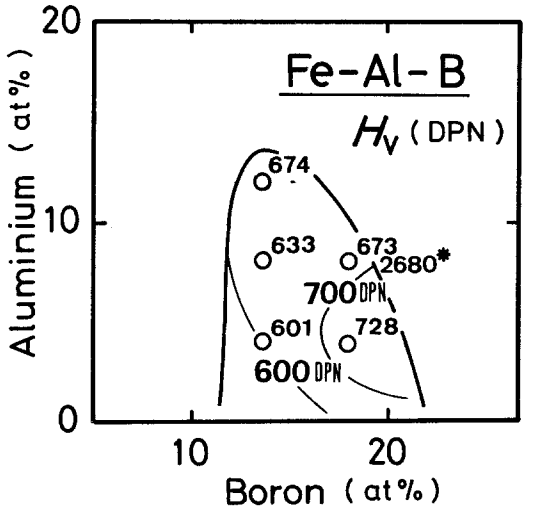

Figure 9 Change in Vickers hardness (H_v) of Fe–Al–B amorphous alloys with alloy composition.

X–Al–B (X = Fe, Co or Ni) alloys, H_v and σ_f decrease in the order iron-, cobalt- to nickel-based alloy, similar to the order of the crystallization temperature.

Ductile–brittle transition behaviour for $X_{74}Al_8B_{18}$ (X = Fe, Co or Ni) amorphous alloys with good bend ductility in the as-quenched state was examined as a function of the ageing time and temperature below 673 K. As an example, their embrittlement behaviour during isothermal ageing at 573 K is shown in Fig. 12, in which the crystallization temperatures are represented for comparison. The strain on the outer surface required for fracture, ϵ_f, is estimated from the equation $\epsilon_f = t/(2r - t)$, where r is the radius of curvature of the bent sample at fracture and t is the thickness of the ribbon specimen. $\epsilon_f = 1$ means that the sample fractured just when $2r = 2t$. The time for beginning of embrittlement is about 10 min for $Fe_{74}Al_8B_{18}$, about 3000 min for $Ni_{74}Al_8B_{18}$ and about 6500 min for $Co_{74}Al_8B_{18}$. To estimate the activation energy for embrittlement (ΔH_f), the relation between the reciprocal of absolute temperature and the logarithmic time at $\epsilon_f = 1$ for $X_{74}Al_8B_{18}$ (X = Fe, Co or Ni) amorphous alloys is plotted in Fig. 13. ΔH_f is about 220 kJ mol^{-1} for $Fe_{74}Al_8B_{18}$, 270 kJ mol^{-1} for $Co_{74}Al_8B_{18}$ and 330 kJ mol^{-1} for $Ni_{74}Al_8B_{18}$. Judging from the time for beginning of embrittlement and the activation energy for embrittlement, it is concluded that the embrittlement tendency of amorphous alloys with ageing depends strongly on the type of parent metal. The iron-based alloy is more susceptible to embrittlement compared with the cobalt- and nickel-based alloys, despite the iron-based alloy possessing the highest crystallization temperature. The same behaviour has been observed in the X–Si–B (X = Fe, Co or Ni) amorphous alloys [9, 10].

3.4. Effect of aluminium on the hardness and crystallization temperature

From Figs 1, 3, 5 and 9 to 11, it is clear that the variation of hardness and crystallization temperature with composition is similar for the three systems examined in the present experiment, namely, these values increase with increasing aluminium or boron content. The increments in

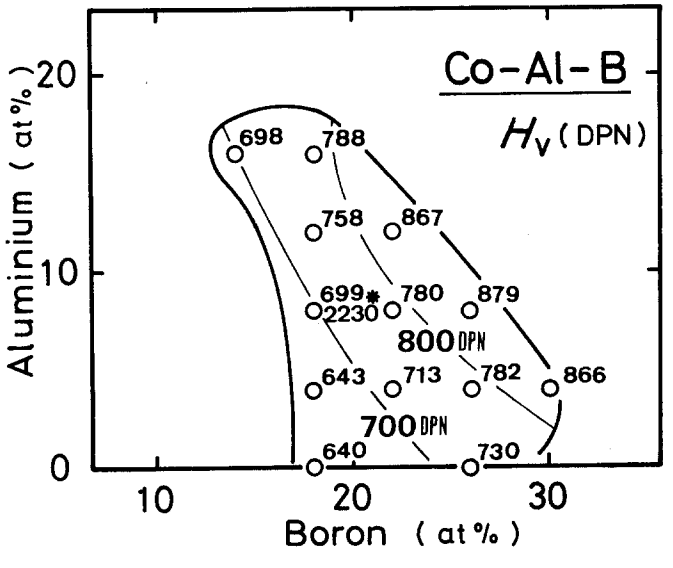

Figure 10 Change in Vickers hardness (H_v) of Co–Al–B amorphous alloys with alloy composition.

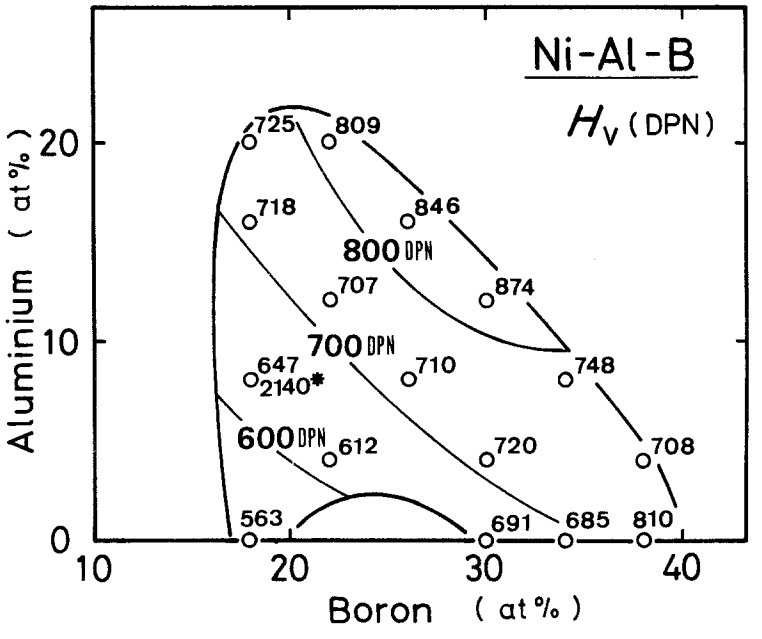

Figure 11 Change in Vickers hardness (H_v) of Ni–Al–B amorphous alloys with alloy composition.

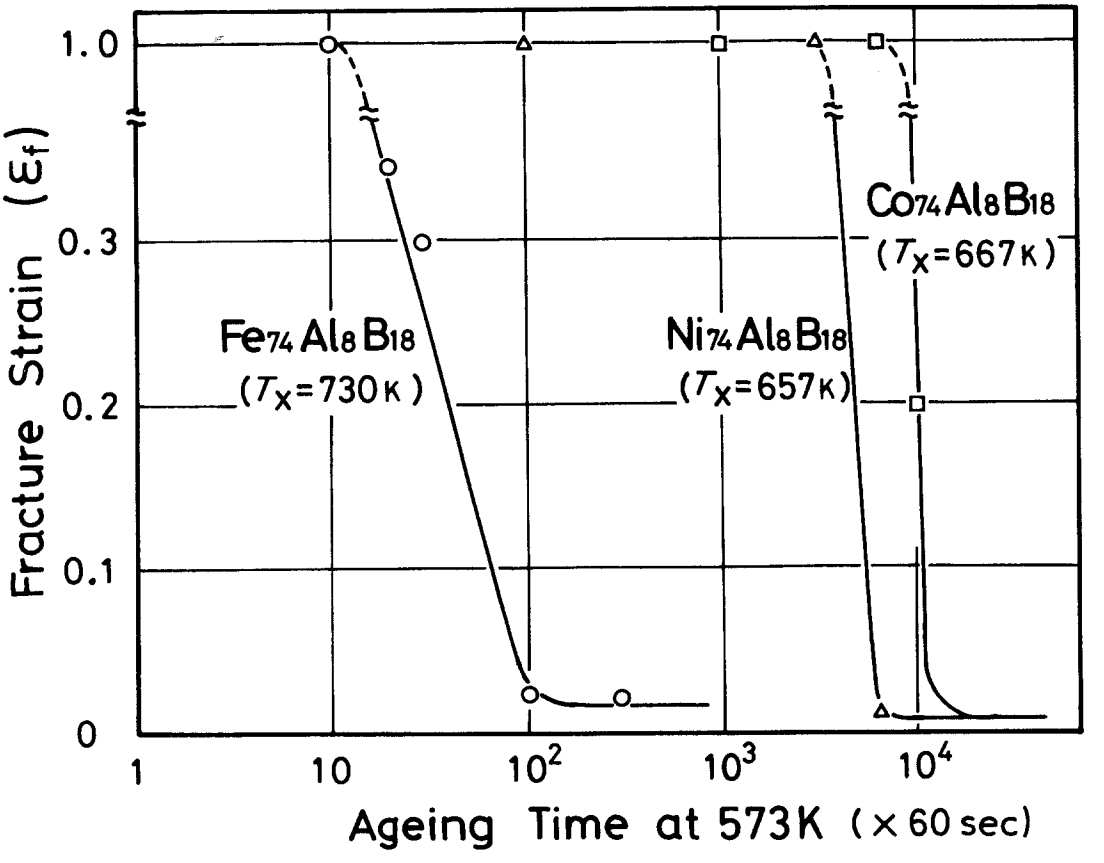

Figure 12 Change in fracture strain of X–Al–B (X = Fe, Co or Ni) amorphous alloys by ageing at 573 K.

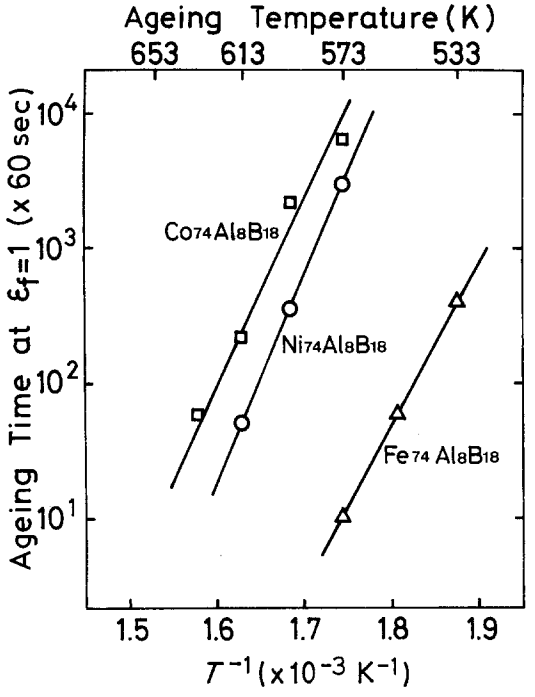

Figure 13 Relationship between the reciprocal of absolute temperature and logarithmic time at $\epsilon_f = 1$ for $X_{74}Al_8B_{18}$ (X = Fe, Co or Ni) amorphous alloys.

these values by the addition of 1 at% aluminium or boron appear to be much greater for boron than for aluminium from the contour of the lines for the hardness and crystallization temperature shown in Figs 1, 3, 5 and 9 to 11. Also, Inoue *et al.* [9, 10] have reported that the hardness and crystallization temperature for X–Si–B (X = Fe, Co or Ni) amorphous alloys shows a larger composition dependence for silicon than for boron. It may be stated from these results that the effectiveness of the three elements on the increase of hardness and crystallization temperature becomes less in the order silicon, boron to aluminium. Additionally, the effectiveness of aluminium on the increase of crystallization temperature was compared with the data on the metalloid effect for iron-based alloys reported by Naka and Masumoto [11]. This result is shown in Fig. 14. As seen in the figure, the effect of metalloids and aluminium on the increase of crystallization temperature decreases in the order of silicon > germanium ≃ carbon > phosphorus > boron > aluminium. Thus, the effect of aluminium is less than that of the metalloids. This result implies that the bonding between iron and aluminium is much weaker than the iron–metalloid bondings as seen by the low hardness value and low decomposition temperature of Fe_3Al compared with Fe_2B, Fe_3C, Fe_3P, Fe_3Si etc. [5, 22, 23]. The weakness may be due to the metal character of aluminium, dissimilar to other metalloid elements. As seen in Figs 1, 3, 5 and 9 to 11, the increase of crystallization temperature and hardness by the addition of aluminium decreases in the order cobalt, nickel to iron systems. It is believed that this order is closely related to the ability of compound formation in each binary system of Fe–Al, Co–Al and Ni–Al.

Additionally, the effect of aluminium on the crystallization temperature and hardness of Fe–B based amorphous alloys was compared with that of alloying elements such as vanadium, chromium, manganese, cobalt and nickel, as shown in Fig. 15. As seen in the figure, aluminium is a more effective element in raising the crystallization temperature and hardness of Fe–B alloys compared with the 4d transition metals except vanadium despite the fact that aluminium is a soft metal with a low melting temperature. This result implies that the bonding of iron–aluminium and/or boron–aluminium is stronger than that of iron–M and/or boron–M for the case of M = manganese, chromium, nickel or cobalt. This tendency is not reasonably explained from the viewpoints of atomic size and electronegativity and the strong bonding for Fe–Al–B amorphous alloys seems to be due to a somewhat metalloid type character of aluminium metal unlike the other transition metals.

4. Summary and conclusions

Amorphous single phases containing a large amount of aluminium have been found in the alloy systems of Fe–Al–B, Co–Al–B and Ni–Al–B by a melt quenching technique. The aluminium content in these amorphous alloys is in the ranges 0 to 60 at% for Fe– and Co–Al–B systems and 0 to 26 at% for the Ni–Al–B system, but the formation of a ductile amorphous phase is limited to less than about 12 at% Al for Fe–Al–B, about 16 at% Al for Co–Al–B and about 20 at% Al for the Ni–Al–B system. The hardness and crystallization temperature of these alloys increase with increasing aluminium and/or boron contents and the highest values attained are about 880 DPN and 887 K. Also, their fracture strengths are about 2140 to 2680 MPa. The effectiveness of aluminium on the increment in hardness and crystallization

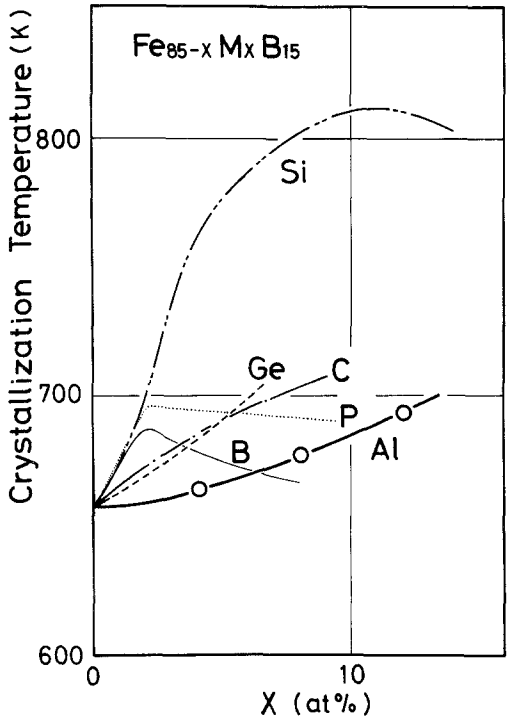

Figure 14 Effects of metalloid elements and aluminium on the crystallization temperature of $Fe_{85}B_{15}$ amorphous alloy.

temperature was compared with the previous data for other metals and metalloids. The effect of aluminium is larger than other metal elements such as chromium, manganese, iron, cobalt and nickel, but is smaller than metalloids such as silicon and boron. Such an order could be reasonably explained by the assumption that aluminium metal may also possess a weak metalloid character. The amorphous phase in $X_{62-78}Al_{8-20}B_{14-18}$ (X = Fe, Co or Ni) ternary alloys crystallizes following the process

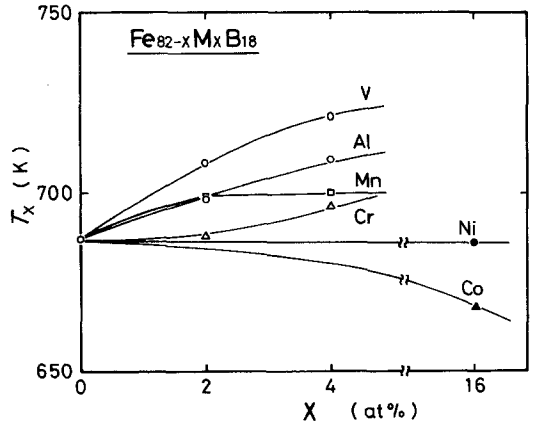

Figure 15 Effect of alloying elements on the crystallization temperature of $Fe_{82}B_{18}$ amorphous alloy.

Amorphous → Amorphous + Crystal-I → Crystal-I + Crystal-II. The first precipitate is a crystal with the same structure as each base metal and the second precipitate is a compound containing large amounts of aluminium and boron.

Acknowledgement

The authors would like to thank Dr C. Suryanarayana of Banaras Hindu University, India (now at The Research Institute for Iron, Steel and Other Metals, Tohoku University) for valuable discussions on the results.

References

1. A. INOUE, Y. KOJIMA, T. MINEMURA and T. MASUMOTO, *Trans. Jap. Inst. Met.* **20** (1979) 468.
2. T. NAOHARA, A. INOUE, T. MINEMURA and T. MASUMOTO, unpublished research (1980).
3. A. KITAMURA, M.Sc. thesis, Tohoku University, 1980.
4. T. MINEMURA, Ph.D. thesis, Tohoku University, 1980.
5. C. J. SMITHELLS, "Metals Reference Book", 5th edn. (Butterworths, London, 1976) pp. 398, 401, 411, 467, 469, 472.
6. H. H. STADELMEIER and R. A. GREGG, *Metal* **16** (1962) 405.
7. H. H. STADELMEIER and A. C. FRAKER, *Z. Metallk.* **53** (1962) 214.
8. A. INOUE, A. KITAMURA and T. MASUMOTO, *Trans. Jap. Inst. Met.* **20** (1979) 404.
9. A. INOUE, T. MASUMOTO, M. KIKUCHI and T. MINEMURA, *J. Jap. Inst. Met.* **42** (1978) 294.
10. *Idem, Sci. Rep. Res. Inst. Tohoku Univ.* **A-27** (1979) 127.
11. M. NAKA and T. MASUMOTO, *ibid.* **A-27** (1979) 118.
12. K. SUZUKI, in "Structure and Properties of Amorphous Metals", edited by T. Masumoto and T. Imura, Supplement to the Sci. Rep. Res. Inst. Tohoku Univ. (1978) p. 1.
13. H. A. DAVIES and J. B. HULL, *J. Mater. Sci.* **11** (1976) 2149.
14. P. RAMACHANDRARAO, M. LARIDJANI and R. W. CAHN, *Z. Metallk.* **63** (1972) 43.
15. T. R. ANANTHARAMAN, P. RAMACHANDRARAO, C. SURYANARAYANA, S. LELE, K. CHATTOPADHYAY, G. V. SASTRY and H. A. DAVIES, "Rapidly Quenched Metals III", Vol. 1, edited by B. Cantor (The Metals Society, London, 1978) p. 126.
16. Y. KOMATSU, M. SHIMOMURA, P. H. SHINGU and R. OZAKI, private communication (1979).
17. H. E. KISSINGER, *Anal. Chem.* **29** (1957) 1702.
18. "Metals Databook", Japan Inst. Metals (Maruzen, Tokyo, 1974) pp. 24–8.
19. T. MASUMOTO, A. INOUE and H. M. KIMURA, *J. Jap. Inst. Met.* **41** (1977) 730.

20. A. INOUE, T. MASUMOTO, S. ARAKAWA and T. IWADACHI, "Rapidly Quenched Metals III", Vol. 1, edited by B. Cantor (The Metals Society, London, 1978) p. 265.
21. R. HILL, "The Mathematical Theory of Plasticity" (Oxford University Press, London, 1967) p. 213.
22. "Metals Databook", The Japan Inst. Metals (Maruzen, Tokyo, 1974) p. 141.
23. C. J. SMITHELLS, "Metals Reference Book", 5th edn (Butterworths, London, 1976) pp. 510, 609, 615.

Received 15 October and accepted 16 December 1980.